# Supplementary Material
# Enhanced generation of non-degenerate photon-pairs in nonlinear metasurfaces

**Matthew Parry**[a,b,*], **Andrea Mazzanti**[c,a], **Alexander Poddubny**[a,d,e], **Giuseppe Della Valle**[c,f], **Dragomir N. Neshev**[a,b], **Andrey A. Sukhorukov**[a,b,†]

[a]Research School of Physics, Australian National University, Canberra, ACT 2601, Australia
[b]ARC Centre of Excellence for Transformative Meta-Optical Systems (TMOS), Australia
[c]Dipartimento di Fisica, Politecnico di Milano, Milan, Italy
[d]ITMO University, 49 Kronverksky Pr., Saint Petersburg 197101, Russia
[e]Ioffe Institute, Saint Petersburg 194021, Russia
[f]Istituto di Fotonica e Nanotecnologie, Consiglio Nazionale delle Ricerche, Milan, Italy

*Matthew Parry, Matthew.Parry@anu.edu.au, †Andrey A. Sukhorukov, Andrey.Sukhorukov@anu.edu.au

# Contents

**S1 Simulation Methods** **1**

**S2 Ghost Oligomers and Symmetry** **2**

**S3 Crystal Orientation** **3**

**S4 SPDC Efficiency** **5**

**S5 Lorentzian Fitting** **7**
S5.1 BIC $\alpha$, gap=52 nm 9
S5.2 BIC $\alpha$, gap=175 nm 11
S5.3 BIC $\beta$, gap=175 nm 14

**S6 Transverse phase-matching in *k*-space** **16**

**S7 Schmidt decomposition** **16**

## S1 Simulation Methods

The simulations were done in COMSOL MultiPhysics, which uses the finite element method, in the Wave Optics module using frequency domain and eigenfrequency studies. Only a single resonator is modeled with the infinite metasurface simulated via Floquet boundaries and infinite space above and below the metasurface by Perfectly Matched Layers. Note that due to the numerical limitations

of the simulation method the infinite quality factors ($Q$) predicted for BICs do not appear, so we take any mode with $Q > 10^3$ in an eigenfrequency study to be worthy of further analysis.

The simulations take into account the material dispersion for AlGaAs over the entire wavelength range considered. We also use an undepleted SFG approximation as this is a condition for quantum-classical correspondence, which allows us to predict the photon-pair rate and construct a wavefunction for SPDC. The signal and idler input fields were generated by as plane waves at specified polar and azimuthal angles. The linear response of the metasurface to the signal and idler beams were calculated separately and the fields of both inside the resonator were used to generate an external current density in a separate SFG simulation. This external current density is shaped by the quadratic nonlinear tensor of AlGaAs and the crystal orientation.

To calculate the farfield SFG power the SFG $\mathbf{E}$ and $\mathbf{H}$ fields are sampled at a plane more than one wavelength from the metasurface. By taking the Fourier transform of these fields we are able to calculate the farfield Poynting vector for each diffraction order. We used a value of second-order nonlinear susceptibility for AlGaAs material as $\chi^{(2)}_{i,j,k} = 200\,\mathrm{pm/V}$ for $i \neq j \neq k$.[35] Our simulations showed that the ratio of the peak SFG power to the peak intensity inside the resonator is relatively constant and so we are able to use the peak signal intensity as a proxy for the farfield SFG power in our initial analyses (See Sec. S4). This greatly reduces the simulation time for initial studies.

## S2 Ghost Oligomers and Symmetry

Because we are interested in nonlinear generation we need to maximize the amount of nonlinear material in the metasurface. We therefore use holes in the material as well as the lattice to determine the group of the metasurface. Because the holes form negative oligomers we have dubbed

them “Ghost Oligomers” since these “Ghosts” drive the behavior of the “body” material. Taking this analogy further we might dub stick and ball meta-atoms “Platonic” since the ghost (stick) is separate from the body (ball), while ghost oligomers would be “Aristotelian” since the ghost and body are inherently inseparable.

With this method we are able to produce all 9 point groups[36] of a 2D repeating pattern, which determines the basis for the eigenmodes that will form in the metasurface. In Fig. S1 for example we see some of the possible ghost oligomer patterns for each of the 9 point groups. Other possibilities are allowed, such as a simple triangular lattice of holes which also has a $D_{6h}$ symmetry. Although this different pattern will have the same basis as that shown in Fig. S1, the different arrangement of the low refractive index air region will mean that the eigenmodes are at different frequencies in the two different patterns. Also, the $D_{6h}$ pattern shown in Fig. S1 has an extra tuning parameter in the gap between the double holes, which allows for greater flexibility in tuning the eigenmodes.

Each group will have its own distinct properties for the dispersion relations which will produce pair rate distributions in $k$-space characteristic of the group. For example, in this study we only calculated one quadrant of $k$-space as the metasurface has $D_{2h}$ symmetry which includes $x$ and $y$ reflection axes. But no cyclic group has reflection axes and hence one would have to calculate all four quadrants to characterize a $C_{1h}$ symmetric metasurface. This is therefore a rich field for future exploration.

## S3 Crystal Orientation

The efficiency of nonlinear frequency conversion in SFG and SPDC processes depends on the crystal structure and orientation. In this paper we study AlGaAs, which has a Zincblende ($\bar{4}3m$)

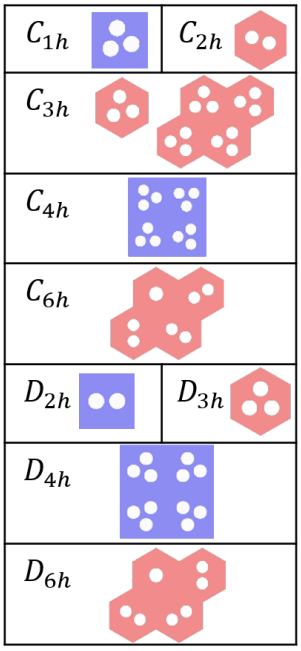


**Fig S1** There are nine point groups for a 2D repeating pattern, all of which can be described with ghost oligomers. The purple designs have a square lattice, while the pink ones have a rhombic lattice.

crystal structure. It has been shown that for Mie modes Zinkblende with (100) orientation has zero SHG emission in the zeroth diffraction order, while both (110) and (111) do have zeroth order emission.[37] It has also been shown that in-plane orientation of the crystal (i.e., in the plane of the metasurface) affects nonlinear emission.[38]

In our simulations the signal and idler are angled to achieve normal emission for the SFG, but at the SFG wavelength there are multiple diffraction orders and so, for convenience, we need a crystal orientation that will give strong emission in the zeroth diffraction order. Our simulations showed that when a BIC is excited every orientation has comparable zeroth order SFG emission. We therefore chose (111) orientation as that also has a strong zeroth emission in the off-BIC illumination and will therefore give a better measure of the enhancement due to the BIC. Our simulations were for SFG from BIC $\alpha$ with $gap = 52$ nm. The SFG wavelength was set to the degenerate (at the BIC) $774.245$ nm and the signal and idler had normal incidence to the metasurface.

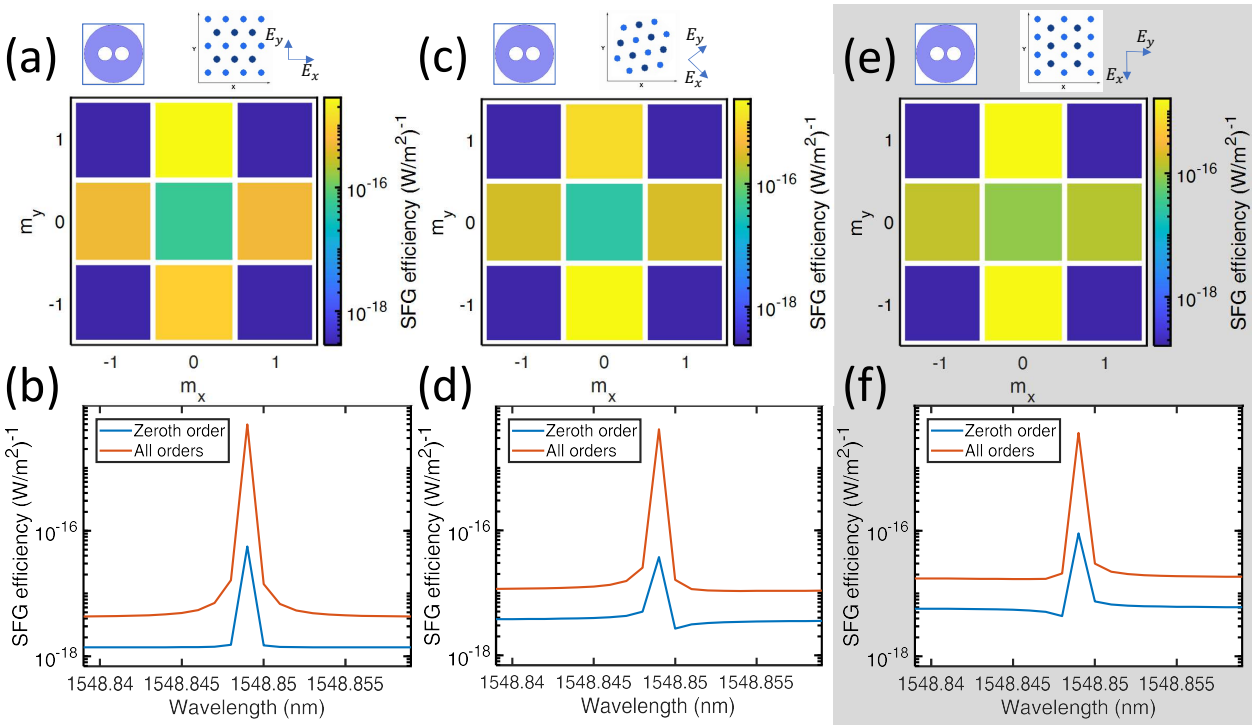


**Fig S2** Farfield SFG efficiency from a (111) oriented AlGaAs crystal by diffraction order when the signal and idler both have vertical polarization. We consider different crystal rotations in the $x$-$y$ plane relative to the meta-atom as illustrated by diagrams at the top: (a,b) (0°), (c,d) 45°, (e,f) 90°. The later orientation used in this paper is highlighted by a gray background. (a,c,e) SFG efficiency at different diffraction orders $(m_x, m_y)$, at the wavelengths corresponding to maximum values in the respective (b,d,f) plots. (b,d,f) The dependence of SFG efficiency in the zeroth order and all orders as indicated by labels on the signal wavelength $\lambda_s$ for a fixed sum-frequency wavelength $\lambda_p = 774.245$ nm.

Because the resonator being studied does not have $\pi/2$ rotation symmetry in the $x$-$y$ plane, the angle of the crystal in this plane will also affect the SFG farfield power. We therefore simulated rotations of the crystal in the $x$-$y$ plane of $0°$, $45°$ and $90°$ - see the results in Fig. S2 where the diagrams at the top show the orientation of the crystal with respect to the meta-atom. The best results were for an $x$-$y$ orientation of $90°$, giving both the highest total efficiency as well as the highest proportion in the zeroth diffraction order as shown in Figs. S2(e) and (f).

## S4 SPDC Efficiency

In our analysis we found that the calculated SPDC rate is approximately proportional to the intensity of the signal and idler fields inside the resonator from our SFG simulations. The justification

for this can be seen in Fig. S3. There are a total of 8 combinations of pump, signal and idler polarization, but the other 3, not shown here or in the letter, are of the same form as those shown. In our work the value for $\Xi_0$ is the ratio of the farfield SFG Poynting vector, corresponding to horizontal or vertical SPDC pump polarization, divided by the product of the maximum intensity of the signal and idler fields inside the resonator. These ratios vary with $\theta$ and $\phi$ so we adopted conservative values. The calculated values are shown in table S1.

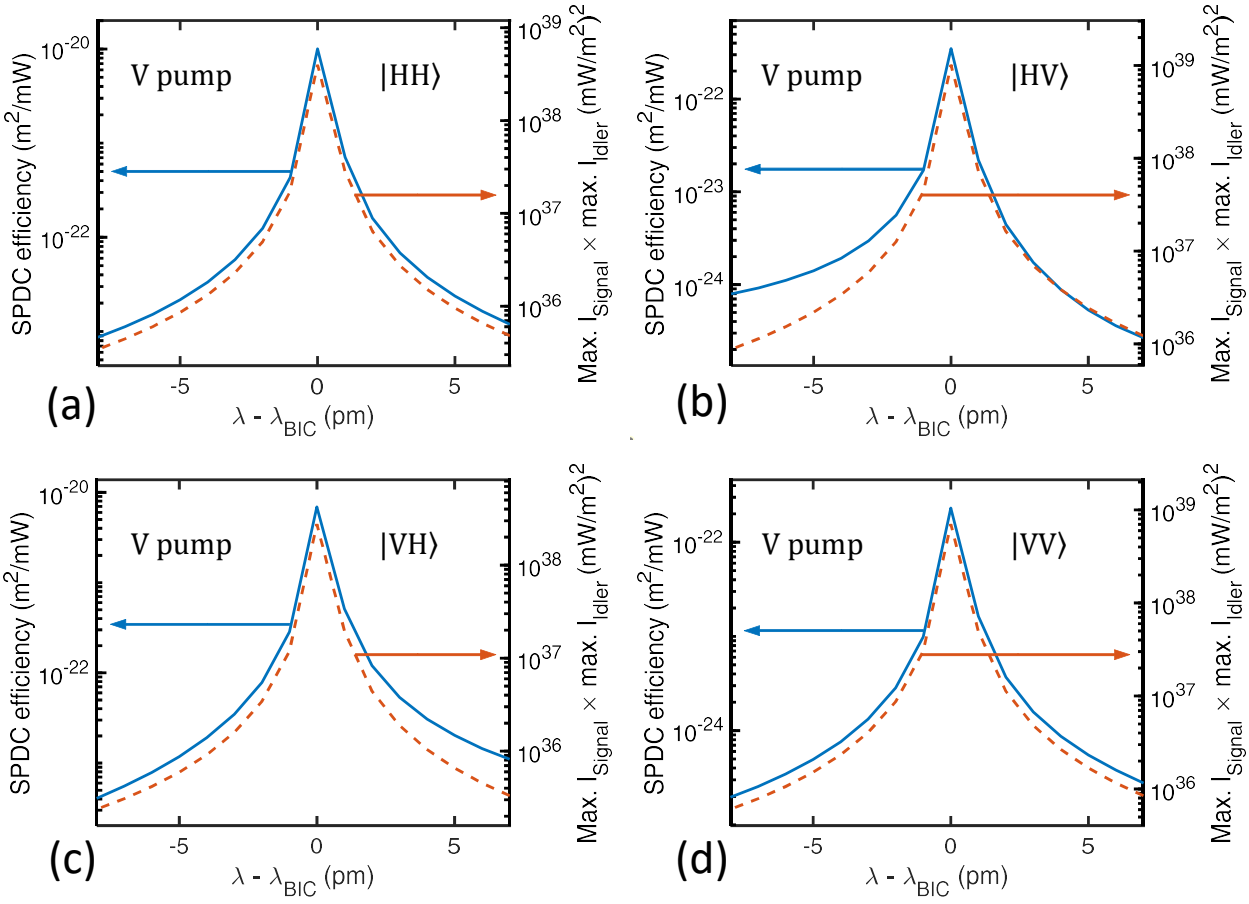


**Fig S3** Comparison between the product of the maximum intensity of the signal and idler in the resonator (dashed lines) and the calculated SPDC rate (solid lines) for BIC $\alpha$ with $gap = 52nm$, $\phi = 79°$ and $\theta_s = 0.2°$ for the signal, opposite angle for the idler, and vertically polarized pump. (a) $|HH\rangle$. (b) $|HV\rangle$. (c) $|VH\rangle$. (d) $|VV\rangle$.

**Table S1** Ratio of the horizontally and vertically polarized components of the SFG farfield intensity at the zeroth diffraction order to the product of maximum signal and idler intensity inside the resonator, in units of $(W/m^2)^{-1}$. 'Degenerate' and 'Non-degenerate' refers to the wavelengths of the signal and idler and signifies the single and double BIC cases respectively.

| | Degenerate | | Non-degenerate | |
|---|---|---|---|---|
| Polariz. signal & idler | Horizontal | Vertical | Horizontal | Vertical |
| $\|HH\rangle$ | $2 \times 10^{-21}$ | $2 \times 10^{-21}$ | $1 \times 10^{-20}$ | $1 \times 10^{-22}$ |
| $\|HV\rangle$ | $3 \times 10^{-21}$ | $3 \times 10^{-23}$ | $2 \times 10^{-20}$ | $2 \times 10^{-24}$ |
| $\|VH\rangle$ | $3 \times 10^{-21}$ | $2 \times 10^{-21}$ | $1 \times 10^{-20}$ | $1 \times 10^{-22}$ |
| $\|VV\rangle$ | $3 \times 10^{-21}$ | $3 \times 10^{-23}$ | $2 \times 10^{-20}$ | $2 \times 10^{-24}$ |

## S5 Lorentzian Fitting

To properly characterize the nonlinear generation we need to determine the $k$-space dependency of each of the parameters determining the BIC lineshape. We therefore ran linear simulations for several angles of the polar ($\theta$) and azimuthal ($\phi$) angles as well as the polarization. We then fitted parameters to the lineshape of the maximum intensity in the resonators and then fitted polynomials in $k$-space to each of these parameters.

In a resonant structure the farfield SFG spectrum should have a Lorentzian lineshape[39] as:

$$\frac{\gamma}{(\omega - \omega_{BIC})^2 + \gamma^2}, \tag{S1}$$

where $\omega$ is the frequency, $\omega_{BIC}$ the peak frequency and $\gamma$ is half of the full width at half maximum. We fitted the following Lorentzian function to our simulation results:

$$L(\omega) = c_1 \left( \frac{\gamma}{(\omega - \omega_{BIC})^2 + \gamma^2} + c_2 \right), \tag{S2}$$

where the background of $c_1 \times c_2$ is not used in subsequent calculations, since it is the enhancement that is significant.

The accuracy of the fitting is characterized by a normalised residual sum of squares defined as

$$R = \frac{\sum (d_{ij} - f(x_i, y_j))^2}{\sum d_{ij}^2},$$

where $f(x_i, y_j)$ is the normalized fitted function and $d_{ij}$ are the data values normalized to the range $0 - 1$. The data is normalized to ensure that the value of $R$ is not affected by the magnitude of the $d_{ij}$. Note that the normalized data is only used in the calculation of $R$ and all other fitting is done with the actual values of the data.

Characteristic examples of the fitted curves $L(\omega)$ are presented in Figs. S4(a) & (b), which show fits for BIC $\alpha$ at $gap = 175$ nm, $\phi = 75°$ and $\theta = 0.1°, 0.45°$ respectively with horizontal polarization. In both cases $R = 8 \times 10^{-8}$. The only cases in which the intensity profile was not Lorentzian was for the six data points (out of 140) of BIC $\alpha$ where $\phi = 0°$, $\theta \geq 0.2°$ and the polarization is horizontal, where typically $R = 10^{-4}$. The enhancement of the field is very low in these cases and so they are not important to our final results for the enhancement of SPDC.

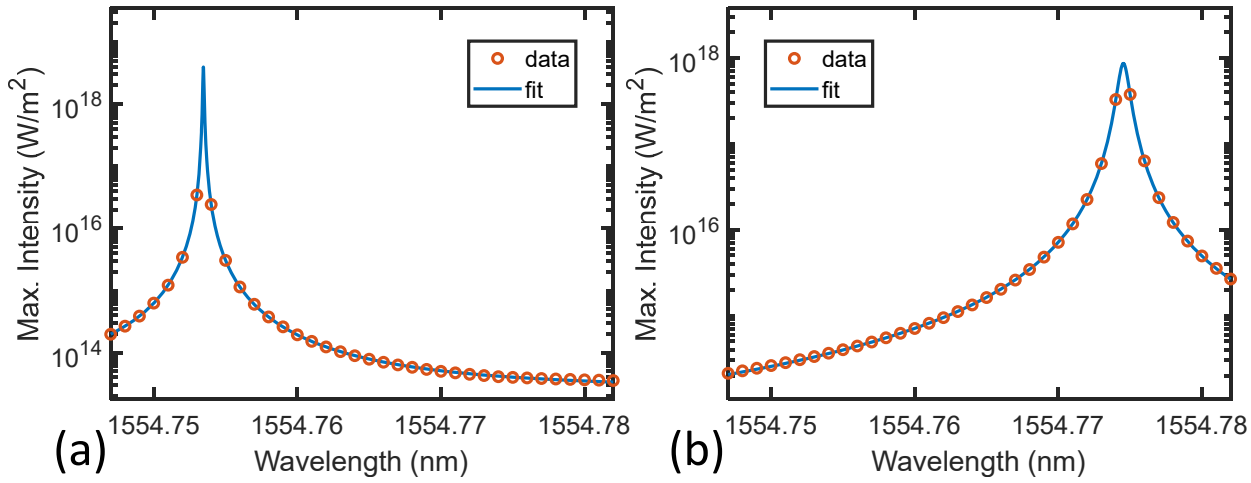


**Fig S4** Lorentzian fitting to simulated maximum intensity in the resonator for BIC $\alpha$ at $gap = 175nm$ with horizontal polarization and $\phi = 75°$. (a) $\theta = 0.1°$, (b) $\theta = 0.45°$.

We then fitted polynomials to the fitted values for $\gamma$, $\omega_{BIC}$ and $c_1$ so that we will have functions

of $\gamma(\mathbf{k})$, $\omega_{BIC}(\mathbf{k})$ and $c_1(\mathbf{k})$. In all of the following results the superscript 'H' indicates results for horizontal polarization and 'V' for vertical polarization.

### *S5.1 BIC $\alpha$, gap=52 nm*

For $\gamma$ we obtained $R^H = 0.0168$ [Fig. S5(a)], $R^V = 0.002$ [Fig. S5(d)] and parabolic fitted functions as expected:

$$\gamma^H(k_x, k_y) = 1.26 \times 10^3\,\mathrm{GHz}\,\mu\mathrm{m}^2\,k_x^2 - 79\,\mathrm{GHz}\,\mu\mathrm{m}^2\,k_y^2 + 1.6 \times 10^{-2}\,\mathrm{GHz},$$

$$\gamma^V(k_x, k_y) = 1.45 \times 10^3\,\mathrm{GHz}\,\mu\mathrm{m}^2\,k_x^2 - 48\,\mathrm{GHz}\,\mu\mathrm{m}^2\,k_y^2 + 2.8 \times 10^{-3}\,\mathrm{GHz}.$$

For $\omega_{BIC}$ we obtained $R^H = 0.0088$ [Fig. S5(b)], $R^V = 8.96 \times 10^{-6}$ [Fig. S5(e)] and with

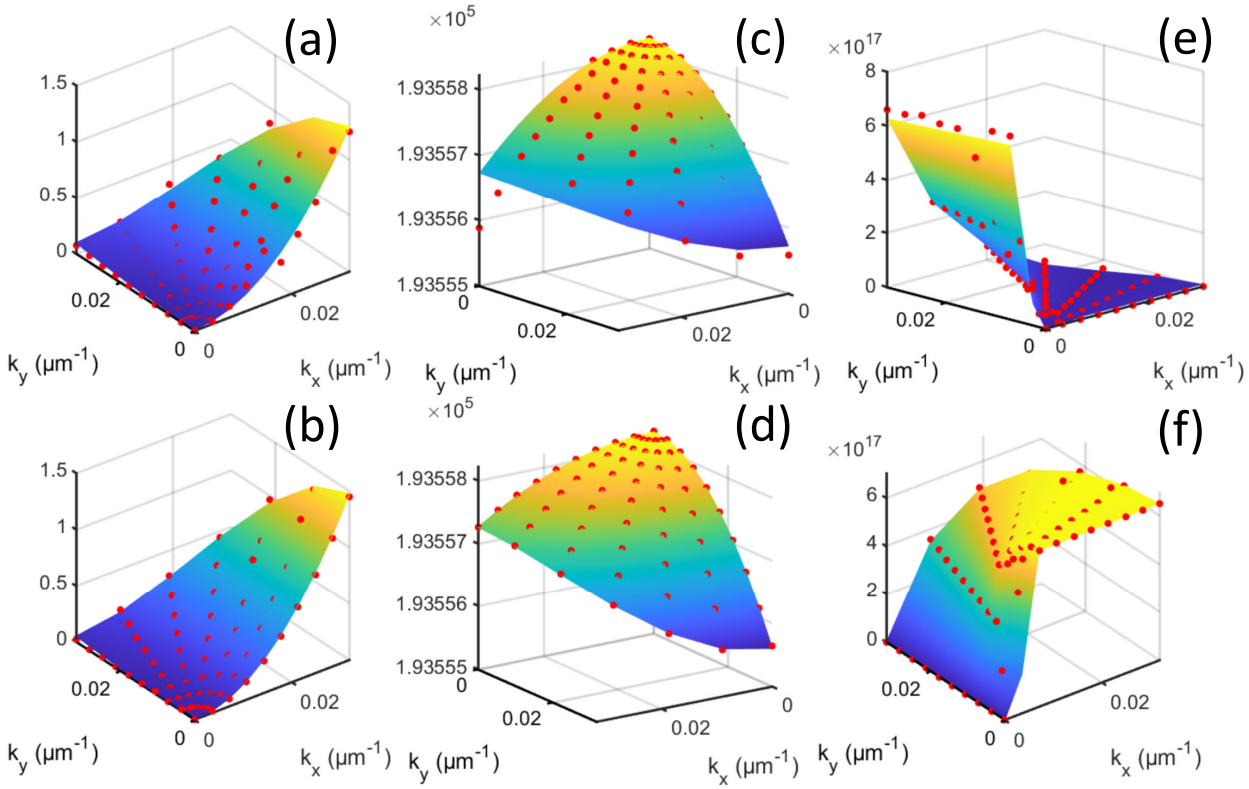


**Fig S5** Lorentzian fitting to simulation results for BIC $\alpha$ with $gap = 52$ nm. The red dots are values fitted to individual simulation results and the surface is the fitted function. (a) $\gamma^H$, (b) $\gamma^V$, (c) $\omega_{BIC}^H$, (d) $\omega_{BIC}^V$, (e) $c_1^H$, (f) $c_1^V$.

fitted functions of

$$\begin{aligned}\omega^{H}_{BIC}(k_x,k_y) &= -1.47\times10^{3}\,\mathrm{GHz}\,\mu\mathrm{m}^2\,k_x^2 - 2.45\times10^{3}\,\mathrm{GHz}\,\mu\mathrm{m}^2\,k_y^2 + 1.9356\times10^{5}\,\mathrm{GHz},\\ \omega^{V}_{BIC}(k_x,k_y) &= -0.93\times10^{3}\,\mathrm{GHz}\,\mu\mathrm{m}^2\,k_x^2 - 2.57\times10^{3}\,\mathrm{GHz}\,\mu\mathrm{m}^2\,k_y^2 + 1.9356\times10^{5}\,\mathrm{GHz}.\end{aligned} \tag{S3}$$

The fitted value for $c_1$ was found to be highly dependent on $\theta$ and $\phi$, with $R^H = 0.0079$ [Fig. S5(c)], $R^V = 0.0478$ [Fig. S5(f)] and fitted functions of

$$\begin{aligned}c_1^H(\theta,\phi) &= \begin{cases}(-1.0101 - 0.1005\,|\theta|)\,g^H(\phi) & \theta \geq 0.1^\circ\\ (10\,\theta)^2\,g^H(\phi) & \theta < 0.1^\circ\end{cases}\\ c_1^V(\theta,\phi) &= \begin{cases}(0.998 + 0.0197\,|\theta|)\,g^V(\phi) & \theta \geq 0.1^\circ\\ (10\,\theta)^2\,g^V(\phi) & \theta < 0.1^\circ\end{cases}\end{aligned} \tag{S4}$$

where

$$\begin{aligned}g^H(\phi) &= 1.22\times10^{10}\,\phi'^4 - 1.98\times10^{13}\,\phi'^2 + 9.77\times10^{15},\\ g^V(\phi_s) &= -1.19\times10^{10}\,\phi'^4 + 1.71\times10^{13}\,\phi'^2 + 6.48\times10^{17},\end{aligned}$$

and to ensure periodicity we have

$$\phi' = \begin{cases}\pi - \phi\ (\mathrm{mod}\ \pi) & \phi\ (\mathrm{mod}\ \pi) > \pi/2\ ,\\ \phi\ (\mathrm{mod}\ \pi) & \phi\ (\mathrm{mod}\ \pi) \leq \pi/2\ .\end{cases}$$

If the polarization is set to whichever value gives the greatest intensity in the resonator then

$c_1(\mathbf{k})$ is constant as expected from Eq. (S1).

### *S5.2 BIC $\alpha$, gap=175 nm*

For $\gamma$ we obtained $R^H = 0.008$ (Fig. S6(a)), $R^V = 0.0011$ (Fig. S6(d)) and parabolic fitted functions as expected:

$$\gamma^H(k_x, k_y) = 685\,\mathrm{GHz}\,\mu\mathrm{m}^2\,k_x^2 - 17\,\mathrm{GHz}\,\mu\mathrm{m}^2\,k_y^2 + 1.5\times10^{-2}\,\mathrm{GHz},$$

$$\gamma^V(k_x, k_y) = 703\,\mathrm{GHz}\,\mu\mathrm{m}^2\,k_x^2 + 0.04\,\mathrm{GHz}\,\mu\mathrm{m}^2\,k_y^2 + 5\times10^{-3}\,\mathrm{GHz}.$$

The fitting is poor along $k_y = 0$, but the enhancement of the SFG is weak here and so this does not affect our results.

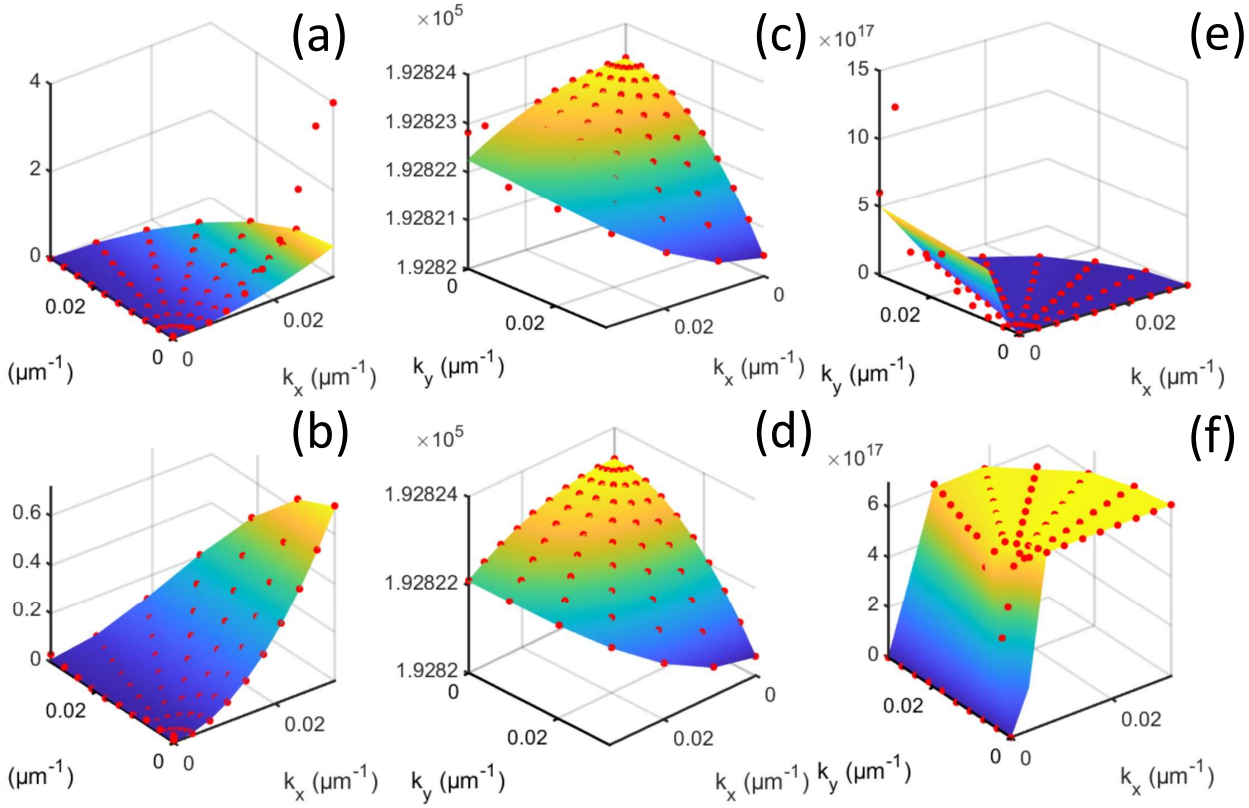


**Fig S6** Lorentzian fitting to simulation results for BIC $\alpha$ with $gap = 175$ nm. The red dots are values fitted to individual simulation results and the surface is the fitted function. (a) $\gamma^H$, (b) $\gamma^V$, (c) $\omega^H_{BIC}$, (d) $\omega^V_{BIC}$, (e) $c_1^H$, (f) $c_1^V$.

For $\omega_{BIC}$ we obtained $R^H = 1.9 \times 10^{-3}$ (Fig. S6(b)), $R^V = 2.9 \times 10^{-7}$ (Fig. S6(e)) and with fitted functions of

$$\begin{aligned}\omega^H_{BIC}(k_x, k_y) &= -1.01 \times 10^3\,\mathrm{GHz}\,\mu\mathrm{m}^2\,k_x^2 - 2.86 \times 10^3\,\mathrm{GHz}\,\mu\mathrm{m}^2\,k_y^2 + 1.9282 \times 10^5\,\mathrm{GHz},\\ \omega^V_{BIC}(k_x, k_y) &= -1.17 \times 10^3\,\mathrm{GHz}\,\mu\mathrm{m}^2\,k_x^2 - 2.84 \times 10^3\,\mathrm{GHz}\,\mu\mathrm{m}^2\,k_y^2 + 1.9282 \times 10^5\,\mathrm{GHz}.\end{aligned} \tag{S5}$$

For $c_1^H$ we get $R^H = 2.3$ [Fig. S6(c)] which, on the face of it, is an unacceptable figure, but which actually demonstrates both the difficulty of automatically fitting such a complicated function and also that the true measure of the fitted polynomials is whether or not they match the simulated data points. The problem we encounter here is that we are not fitting polynomials to data points, but rather we are fitting polynomials to data that is itself fitted to data points. That is, the first fitting creates the values of $\gamma$ and $c_1$ from the simulation data. Thus if $\gamma$ is a little larger in the fitting then $c_1$ will be correspondingly smaller and we should not be surprised if a variability of less than an order of magnitude occurs where $\gamma$ is very small and thus more prone to proportional variation. However the second fitting, which creates the polynomials, smooths out these variations in $\gamma$ and we therefore need to be careful not to create a polynomial for $c_1$ that has features not present in the simulation data. The true measure of the success of the fitting is therefore not how well an individual polynomial fits the fitted data, but how well the combinations of the polynomials in the Eq. (S2) matches the simulations.

A further difficulty is introduced by the fact that the simulations are done at discrete frequencies and since a quasi-BIC has an extremely high quality factor, the maximum intensity and thus the SFG produced will depend strongly on the wavelength of the simulation point that is closest to the BIC maximum. Computational limitations mean that we can not do simulations arbitrarily close to

such high quality factor resonance peaks. There is therefore no single numerical measure that will give a perfect measure of the goodness of the fit and we must therefore exercise some judgment in choosing fitting functions. This convergence of factors forced us to ignore $R^H$ in this case and instead have chosen a fitted function for $c_1^H$ that complements $c_1^V$ in the same way that they do in Eq. (S4), as illustrated in Figs. S5(e) & (f).

In the vertical case we obtained $R^V = 0.049$ [Fig. S6(f)] and fitted functions for horizontal and vertical cases of

$$c_1^H(\theta,\phi) = \begin{cases} (0.9 + 0.98\,|\theta|)\, g^H(\phi) & \theta \geq 0.1^\circ \\ (100\,\theta^2)\, g^H(\phi) & \theta < 0.1^\circ \end{cases}$$

$$c_1^V(\theta,\phi) = \begin{cases} (-1.0003 + 0.002\,|\theta|)\, g^V(\phi) & \theta \geq 0.1^\circ \\ (-100\,\theta^2)\, g^V(\phi) & \theta < 0.1^\circ \end{cases}$$

where

$$g^H(\phi) = 1.4\times10^9\,\phi'^5 - 2.5\times10^{11}\,\phi'^4 + 1.6\times10^{13}\,\phi'^3 - 4.0\times10^{14}\,\phi'^2 + 3.3\times10^{15}\,\phi' - 2.3\times10^{14}$$

$$g^V(\phi_s) = 2.8\times10^9\,\phi'^5 - 4.9\times10^{11}\,\phi'^4 + 3.1\times10^{13}\,\phi'^3 - 7.8\times10^{14}\,\phi'^2 + 6.5\times10^{15}\,\phi' - 6.8\times10^{17}$$

and to ensure periodicity we have

$$\phi' = \begin{cases} \pi - \phi \,(\mathrm{mod}\,\pi) & \phi \,(\mathrm{mod}\,\pi) > \pi/2 \,, \\ \phi \,(\mathrm{mod}\,\pi) & \phi \,(\mathrm{mod}\,\pi) \leq \pi/2 \,. \end{cases}$$

*S5.3 BIC $\beta$, gap=175 nm*

For $\gamma$ we obtained $R^H = 0.0038$ [Fig. S7(a)], $R^V = 0.0015$ [Fig. S7(d)] and parabolic fitted functions as expected:

$$\gamma^H(k_x, k_y) = -1.45\,\mathrm{GHz}\,\mu\mathrm{m}^2\,k_x^2 + 131\,\mathrm{GHz}\,\mu\mathrm{m}^2\,k_y^2 + 5\times10^{-3}\,\mathrm{GHz},$$
$$\gamma^V(k_x, k_y) = -0.7\,\mathrm{GHz}\,\mu\mathrm{m}^2\,k_x^2 + 135\,\mathrm{GHz}\,\mu\mathrm{m}^2\,k_y^2 + 2.7\times10^{-3}\,\mathrm{GHz}.$$

For $\omega_{BIC}$ we obtained $R^H = 1.1\times10^{-6}$ [Fig. S7(b)], $R^V = 1.9\times10^{-7}$ [Fig. S7(e)] and with fitted functions of

$$\begin{aligned} \omega^H_{BIC}(k_x, k_y) &= 1.6\times10^3\,\mathrm{GHz}\,\mu\mathrm{m}^2\,k_x^2 + 1.8\times10^3\,\mathrm{GHz}\,\mu\mathrm{m}^2\,k_y^2 + 1.944\times10^5\,\mathrm{GHz}, \\ \omega^V_{BIC}(k_x, k_y) &= 1.6\times10^3\,\mathrm{GHz}\,\mu\mathrm{m}^2\,k_x^2 + 1.8\times10^3\,\mathrm{GHz}\,\mu\mathrm{m}^2\,k_y^2 + 1.944\times10^5\,\mathrm{GHz}. \end{aligned} \tag{S6}$$

For $c_1$ we get $R^H = 0.21$ and $R^V = 2.6$ [Fig. S7(f)] where we have had to use the same

procedure as with $c_1^H$ in Sec. S5.2. The fitted functions are

$$c_1^H(\theta,\phi) = \begin{cases} (0.96 + 0.40\,|\theta|)\, g^H(\phi) & \theta \geq 0.1^\circ \\ (100\,\theta^2)\, g^H(\phi) & \theta < 0.1^\circ \end{cases}$$

$$c_1^V(\theta,\phi) = \begin{cases} (1 - 5.9\times 10^{-16}\,|\theta|)\, g^V(\phi) & \theta \geq 0.1^\circ \\ (-100\,\theta^2)\, g^V(\phi) & \theta < 0.1^\circ \end{cases}$$

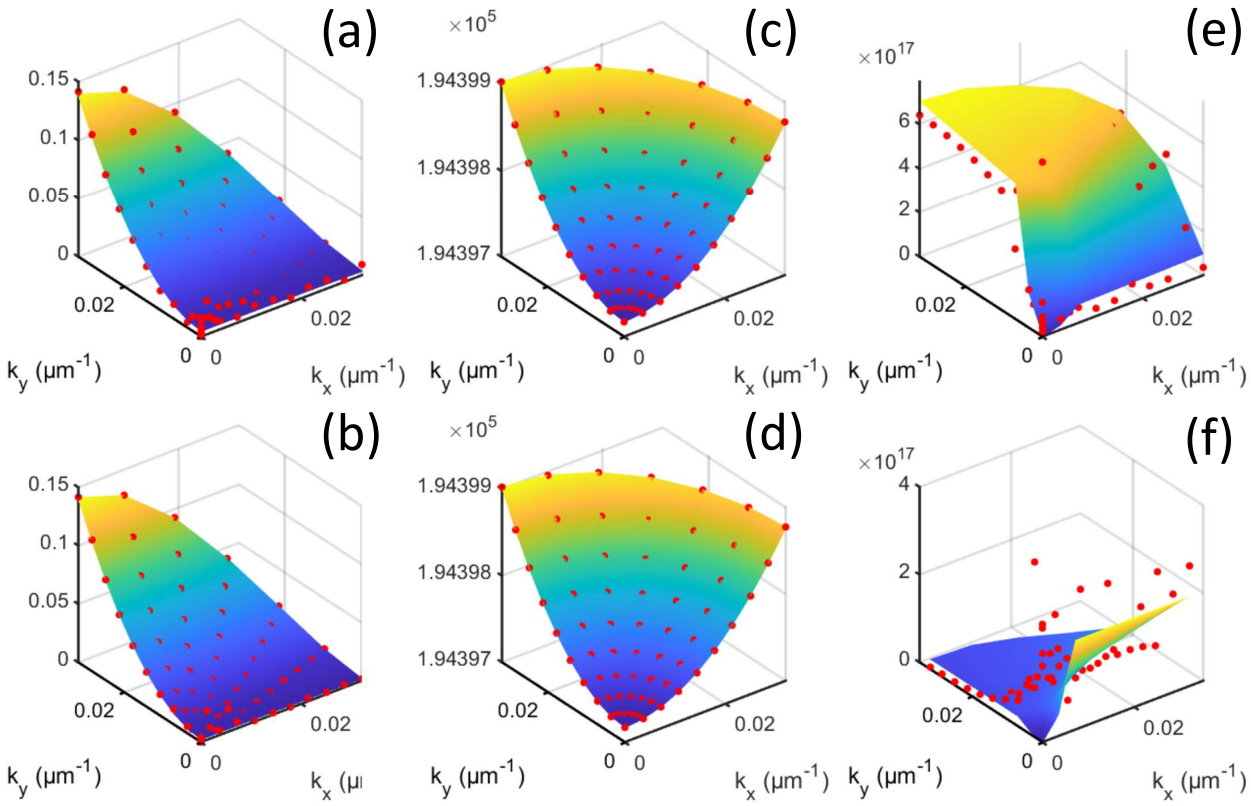


**Fig S7** Lorentzian fitting to simulation results for BIC $\beta$ with $gap = 175$ nm. The red dots are values fitted to individual simulation results and the surface is the fitted function. (a) $\gamma^H$, (b) $\gamma^V$, (c) $\omega_{BIC}^H$, (d) $\omega_{BIC}^V$, (e) $c_1^H$, (f) $c_1^V$.

where

$$g^H(\phi) = -5.7 \times 10^8\, \phi'^5 + 1.2 \times 10^{11}\, \phi'^4 - 7.0 \times 10^{12}\, \phi'^3 - 1.0 \times 10^{14}\, \phi'^2 + 2.1 \times 10^{16}\, \phi' + 8.4 \times 10^{16}$$

$$g^V(\phi_s) = 2.6 \times 10^8\, \phi'^4 + 4.0 \times 10^{11}\, \phi'^3 - 9.4 \times 10^{13}\, \phi'^2 + 7.1 \times 10^{15}\, \phi' - 2.1 \times 10^{17}$$

and to ensure periodicity we have

$$\phi' = \begin{cases} \pi - \phi \,(\mathrm{mod}\, \pi) & \phi \,(\mathrm{mod}\, \pi) > \pi/2\ , \\ \phi \,(\mathrm{mod}\, \pi) & \phi \,(\mathrm{mod}\, \pi) \leq \pi/2\ . \end{cases}$$

## S6 Transverse phase-matching in *k*-space

The form of the dispersion for each BIC depends on the polarization of the signal and idler and so there is some variation in the transverse phase matching condition for each polarization combination, as shown in Fig. S8. For the cases studied in this paper the variations occur in regions of $k$-space with relatively low generation rates and hence it does not affect our results.

## S7 Schmidt decomposition

In our case the Schmidt decomposition[40] is a form of Singular Value Decomposition (SVD). Specifically, an $m \times n$ matrix $M$, with $m > n$, can be decomposed into the three matrices $U$, $\Lambda$ and $V$ as

$$M = U\Lambda V^*,$$

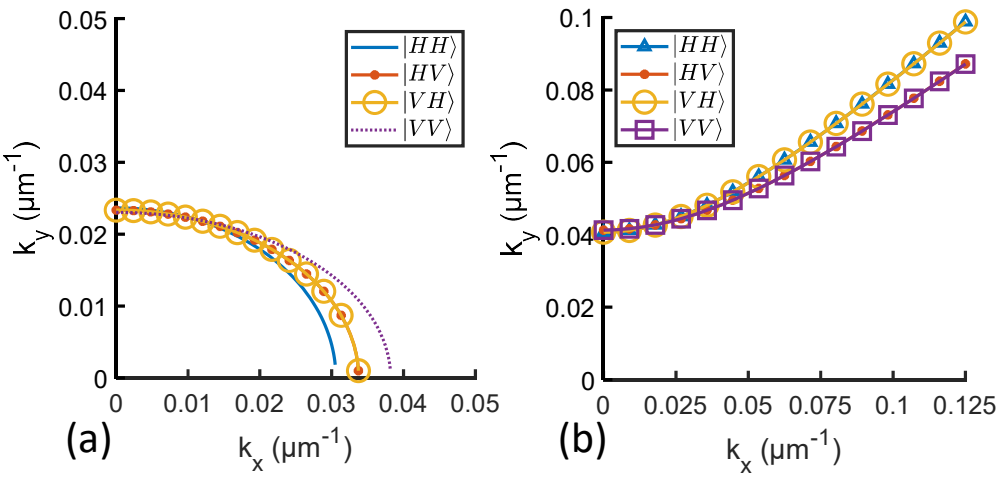


**Fig S8** The angle in $k$-space at which $\omega_p(\mathbf{k}_{p,\perp}) = \omega_s(\mathbf{k}_{s,\perp}) + \omega_i(\mathbf{k}_{i,\perp})$ for different polarizations of the signal and idler. (a) Single BIC case, $\lambda_p = 774.43$ nm. (b) Two BIC case, $\lambda_p = 774.22$ nm. Note that the curves are hyperbolic in this case.

where $U$ and $V$ are unitary (i.e., their column vectors are orthonormal) and $\Lambda$ is diagonal and positive real. In quantum mechanics it is more convenient to write

$$\Lambda = \left[\lambda_{qq}\right] \equiv \left[\sqrt{\lambda_q}\right].$$

We can then derive the result

$$\begin{aligned} M = [m_{ij}] &= \left[u_{iq}\sqrt{\lambda_q}\right] V^* \\ &= \left[\sum_q u_{iq}\sqrt{\lambda_q}\overline{v}_{jq}\right] \\ &= \sum_q \sqrt{\lambda_q}[u_{iq}\overline{v}_{jq}] \\ &= \sum_q \sqrt{\lambda_q}\,|u_q\rangle \otimes |v_q\rangle\,, \end{aligned} \tag{S7}$$

where $\sqrt{\lambda_q} \in \mathbb{R}$ and $\otimes$ is the outer product. To understand the importance of this result we need to view the matrix $M$ as a linear map from one vector space to another. Now, not every $M$ will

be diagonalizable if we use the same basis for both vector spaces. However in Eq. (S7) we have shown that $M$ is *always* diagonalizable if we use different bases, $\{|u_q\rangle\}$ and $\{|v_q\rangle\}$, for the two vector spaces.[41]

With SPDC we have two particles, the signal and idler photons, with Hilbert spaces of $\mathscr{H}_s$ and $\mathscr{H}_i$, and so the wavefunction will exist in the tensor product of these two spaces: $\mathscr{H}_s \otimes \mathscr{H}_i$. By using the standard Jones vectors of

$$|H\rangle = \begin{bmatrix} 1 \\ \\ 0 \end{bmatrix}, \quad \text{and} \quad |V\rangle = \begin{bmatrix} 0 \\ \\ 1 \end{bmatrix},$$

we constructed a wavefunction of

$$\begin{aligned} |\Psi\rangle =& \sqrt{A}\big(E^{HH}\,|H\rangle \otimes |H\rangle + E^{HV}\,|H\rangle \otimes |V\rangle + E^{VH}\,|V\rangle \otimes |H\rangle + E^{VV}\,|V\rangle \otimes |V\rangle\big) \\ =& \sqrt{A} \begin{bmatrix} E^{HH} & E^{HV} \\ \\ E^{VH} & E^{VV} \end{bmatrix}, \end{aligned}$$

where $E^{HV}$ is the farfield $\mathbf{E}$ for the inverse process of Sum Frequency Generation (SFG) when the signal beam has horizontal polarization and the idler beam has vertical polarization, and $A$ is a normalization factor. That is, we started by using the same basis, $\{|H\rangle, |V\rangle\}$, for both of the Hilbert spaces ($\mathscr{H}_s$ and $\mathscr{H}_i$).

With SVD we generated two $2 \times 2$ matrices of

$$U = \begin{bmatrix} |u_1\rangle & |u_2\rangle \end{bmatrix} \quad \text{and} \quad V = \begin{bmatrix} |v_1\rangle & |v_2\rangle \end{bmatrix},$$

which we used as the bases $\{|u_1\rangle, |u_2\rangle\}$ for $\mathscr{H}_s$ and $\{|v_1\rangle, |v_2\rangle\}$ for $\mathscr{H}_i$. By using the Schmidt parameters $\sqrt{\lambda_1}$ and $\sqrt{\lambda_2}$ we can then express the wavefunction in terms of these new bases as

$$|\Psi\rangle = \sqrt{\lambda_1}\,|u_1\rangle \otimes |v_1\rangle + \sqrt{\lambda_2}\,|u_2\rangle \otimes |v_2\rangle\,. \tag{S8}$$

We have therefore created a custom basis of $\mathscr{H}_s \otimes \mathscr{H}_i$ for the particular state $|\Psi\rangle$ which will express this state as simply as possible.

From this diagonalized form of $|\Psi\rangle$ in Eq. (S8) we can immediately see that if there is more than one non-zero Schmidt parameter then there will be entanglement between the signal and idler. We can also quantify the degree of entanglement with the Schmidt number[40]

$$K = \frac{1}{\sum_q \lambda_q^2}$$

where the minimum value of 1 indicates no entanglement. The maximum value of $K = n$ occurs when all of the Schmidt parameters have the same value of $\sqrt{\lambda_q} = 1/\sqrt{n}$.

We can determine the dependence of the entanglement on the polarization of the pump by constructing a wavefunction from one polarization of the SFG E farfield only, i.e.

$$|\Psi_H\rangle = \sqrt{A}\begin{bmatrix} E_x^{HH} & E_x^{HV} \\ E_x^{VH} & E_x^{VV} \end{bmatrix},$$

and likewise for vertical polarization. To get the wavefunction for an arbitrary linear polarization we apply a linear polarizer $L(\psi)$ at angle $\psi$ from the horizontal to the SFG E farfield and then rotate the axes to align them with the polarizer. From this polarization we can then get an arbitrary elllip-

ticity by rotating by an angle of $\chi$ from the $\hat{S}_1$–$\hat{S}_2$ polarization plane about an axis perpendicular to $L(\psi)$ via

$$R_{\hat{n}}(\chi)L(\psi)R_{\hat{n}}(-\chi),$$

where[42]

$$R_{\hat{n}}(\chi) = \exp(-i\chi\hat{n}\cdot\vec{\sigma})$$

$$\hat{n} = R(2\psi - \pi/2)\begin{bmatrix}1\\0\end{bmatrix}$$

and

$$\vec{\sigma} = -\sigma_3\hat{S}_1 + \sigma_1\hat{S}_2$$

has been modified to account for the different orientation of the axes on the Poincaré sphere relative to the Bloch sphere. After rotating the axes to match the new polarization the operation can be expressed as

$$\begin{bmatrix}1 & 0\\0 & 0\end{bmatrix} R(-\psi)R_{\hat{n}}(-\chi)\begin{bmatrix}E_x\\E_y\end{bmatrix} = \begin{bmatrix}E_{\psi,\chi}\\0\end{bmatrix},$$

which is physically equivalent to rotating the E field in the opposite sense and applying a horizontal polarizer.

# List of Figures

S1 Examples of Ghost Oligomer metasurfaces

S2 Farfield SFG efficiency

S3 SPDC efficiency vs max. intensity in resonator

S4 Lorentzian fitting examples

S5 Polynomial fitting for BIC $\alpha$ with $gap = 52$ nm

S6 Polynomial fitting for BIC $\alpha$ with $gap = 175$ nm

S7 Polynomial fitting for BIC $\beta$ with $gap = 175$ nm

S8 Polarisation dependence of transverse phase matching

# List of Tables

S1 SFG efficiency